than 2000°C (thus, for instance, the microwave drill has failed to penetrate into sapphire). To accelerate the thermal-runaway process, the material properties should be dependent on temperature in a way that the dielectric loss increases and/or the thermal conductivity decreases with increasing temperature. A positive temperature dependence of the dielectric losses characterizes many nonconductive materials (*12–14*). This feature increases the microwave power absorption in the evolved hot spot and therefore accelerates the temperature growth-rate and the thermal-runaway process. A preheating of such materials may also assist the microwave-drill operation.

Owing to thermal stresses, the microwave-drill operation on brittle materials such as silicon and glass may cause cracks (these were observed by optical and scanning-electron microscopes in ranges of 1 to 2 mm around some of the holes). This problem could be alleviated by a more gradual operation or by preheating. For larger holes, the affected zone could be removed mechanically during the microwave-drilling process. It should be noted, however, that in ceramics and aggregated materials the microwave drill may add a local sintering-like effect, and thus the material forming the walls may be strengthened.

Safety considerations impose certain limitations on the microwave drill operation, such as shielding to comply with safety standards. This could be implemented either by using a closed chamber (such as the domestic oven) or an open shielding plate (as illustrated in Fig. 1). The closed structure is applicable for automatic production lines, whereas the open shield may fit in construction and geological works. Both solutions were tested and resulted in <1 mW/cm^2 microwave power-density leakage, in accordance with common safety standards.

A comparison of the microwave-drill concept to mature drilling technologies is shown in Table 1 for mechanical and laser-based drills. The microwave drill integrates electromagnetic-radiation, heating, and mechanical effects, and in this sense it can be regarded as a hybrid method. However, unlike mechanical drills, the microwave-drill operation is quiet and clean. It does not contain fast rotating parts, nor does it cause mechanical friction, and its operation is essentially dust-free. On the other hand, the microwave drill emits hazardous radiation, which requires safety measures and limits its operating conditions.

The microwave-drill concept is not expected to compete with laser-based drills in accurate industrial tasks, but it should provide a low-cost solution for a variety of needs for holes in the millimeter-to-centimeter diameter range in common materials such as concrete, rocks, ceramics, silicates, and glasses. The microwave drill may find applications in industrial production lines, professional drilling-tools, and construction and geological equipment. It may also be most effective in low-cost applications that require silent, clean, and efficient operation.

References and Notes

1. K. Krajick, *Science* **283**, 781 (1999).
2. J. F. Ready, *Industrial Applications of Lasers* (Academic Press, New York, 1997).
3. J. Thuery, *Microwave: Industrial, Scientific, and Medical Applications* (Artech House, Boston, 1992).
4. D. P. Lindroth, R. J. Morrell, J. R. Blair, U.S. Patent 5,003,144 (1991).
5. A. C. Metaxas, *Foundations of Electroheat—A Unified Approach* (Wiley, Chichester, UK, 1996).
6. P. E. Parris, V. M. Kenkre, *Phys. Status Solidi (b) Basic Res.* **200**, 39 (1997).
7. C. A. Vriezinga, *J. Appl. Phys.* **83**, 438 (1998).
8. E. Jerby, V. Dikhtyar, U.S. Patent 6,114,676 (2000).
9. U. Grosglick, V. Dikhtyar, E. Jerby, paper presented at the European Symposium on Numerical Methods in Electromagnetics, (JEE'02), Toulouse, France, 6 to 8 March 2002.
10. Y. Alpert, E. Jerby, *IEEE Trans. Plasma Sci.* **27**, 555 (1999).
11. R. W. P. King, C. W. Harrison, *Antennas and Waves: A Modern Approach* (MIT Press, Cambridge, MA, 1969).
12. N. G. Evans, M. G. Hamlyn, *Mater. Res. Soc. Symp. Proc.* **430**, 9 (1996).
13. R. M. Hutcheon *et al.*, *Mater. Res. Soc. Symp. Proc.* **269**, 541 (1992).
14. A. Birnboim *et al.*, *J. Am. Ceram. Soc.* **81**, 1493 (1998).

15. We acknowledge the support of the State-of-Israel Ministry of National Infrastructures, the Belfer Foundation, and the Schechterman Foundation.

24 April 2002; accepted 11 September 2002

Kilimanjaro Ice Core Records: Evidence of Holocene Climate Change in Tropical Africa

Lonnie G. Thompson,[1,2]* Ellen Mosley-Thompson,[1,3] Mary E. Davis,[1,2] Keith A. Henderson,[1,2] Henry H. Brecher,[1] Victor S. Zagorodnov,[1,2] Tracy A. Mashiotta,[1] Ping-Nan Lin,[1] Vladimir N. Mikhalenko,[4] Douglas R. Hardy,[5] Jürg Beer[6]

Six ice cores from Kilimanjaro provide an ~11.7-thousand-year record of Holocene climate and environmental variability for eastern equatorial Africa, including three periods of abrupt climate change: ~8.3, ~5.2, and ~4 thousand years ago (ka). The latter is coincident with the "First Dark Age," the period of the greatest historically recorded drought in tropical Africa. Variable deposition of F^- and Na^+ during the African Humid Period suggests rapidly fluctuating lake levels between ~11.7 and 4 ka. Over the 20th century, the areal extent of Kilimanjaro's ice fields has decreased ~80%, and if current climatological conditions persist, the remaining ice fields are likely to disappear between 2015 and 2020.

Few continuous, high-temporal-resolution climate histories are available from the tropics, although climate variability in this region strongly forces the global climate system. A modest number of ice core records exist for South America, the Himalayas, and the Tibetan Plateau, and here we present the first ice core–based climate history for Africa, recovered from the ice fields atop Kilimanjaro. In January and February of 2000, six ice cores (Fig. 1) were drilled to bedrock on three remnant ice fields on the rim and summit plateau of Kilimanjaro (3°04.6′S; 37°21.2′E; 5893 m above sea level). These cores provide the last opportunity to establish an ice core record of African climate. The three longest cores (NIF1, NIF2, and NIF3) were drilled to depths of 50.9, 50.8, and 49.0 m, respectively, from the Northern Ice Field (NIF), the largest of the ice bodies. Two shorter cores (SIF1 and SIF2) were drilled to bedrock on the Southern Ice Field (SIF) to depths of 18.5 and 22.3 m, respectively, and a 9.5-m core was drilled to bedrock on the small, thin Furtwängler Glacier (FWG) within the crater. Temperatures were measured in each borehole; in the NIF, they ranged from −1.2°C at 10 m depth to −0.4°C at bedrock, and in the SIF, they were near 0°C. No evidence of water was observed in the boreholes on the NIF or SIF, but the FWG was water-saturated throughout. Sampling and analysis details are provided in the supporting online text.

Aerial photographs taken on 16 February 2000 allowed production of a recent detailed map of ice cover extent on the summit plateau (Fig. 1). Concurrent with the drilling program,

[1]Byrd Polar Research Center, [2]Department of Geological Sciences, [3]Department of Geography, The Ohio State University, Columbus, OH 43210, USA. [4]Institute of Geography, Moscow, Russia. [5]Department of Geosciences, University of Massachusetts, Amherst, MA 01003–9297, USA. [6]Swiss Federal Institute for Environmental Science and Technology (EAWAG) Duebendorf, Switzerland.

*To whom correspondence should be addressed. E-mail: thompson.3@osu.edu

an automatic weather station (AWS) was established at the NIF2 drill site (5794 m above sea level; 506 hectopascals) to measure aspirated air temperature and humidity, incoming solar radiation, wind speed and direction, barometric pressure, and changes in the surface height by either accumulation or ablation (*1*). Two years of AWS observations revealed that daily air temperatures varied only slightly about the annual mean (–7.1°C) throughout the year and that daily temperature maxima remained below –2°C. The predominant airflow was from the east-southeast (~75% of hourly values) and wind direction remained steady for months at a time. Precipitation occurred during all months, always as snow, with monthly totals typically less than 100 mm and a distribution that generally followed the bimodal precipitation pattern of the region. In 2000, 51% of the precipitation fell between March and May, the season of the long rains (*2*).

Accumulation stakes placed on the tops of the three ice fields and along the front of the crater-side wall of the NIF in February 2000 were remeasured in February 2001. The surfaces of the NIF, FWG, and SIF had lowered by 1.09 m, 0.64 m, and 1.08 m, respectively, removing the most recent stratigraphic layers and the climate records they contained. In addition, measurement of the three stakes placed in front of the vertical walls on the crater side of the NIF confirmed an annual average retreat of ~0.92 m (from 2000 to 2002), suggesting that the position of the ice edge varies through time. These observations, coupled with the meteorological observations for 2001 and 2002, document a loss of ~0.93 m water equivalent (w.e.) from 2000 to 2001 and a positive balance of ~0.13 m w.e. from 2001 to 2002 for the NIF surface.

A compilation of five maps of ice extent since 1912, the first four assembled by Hastenrath and Greischar (*3*), demonstrates a sustained loss of ice on Kilimanjaro over the past century (Fig. 1). An independent check on the 1976 ice extent (*4*) also included a map compiling observations between 1887 and 1898. Maps and digital elevation models of ice boundaries and ice elevations were produced from stereoscopic aerial photo coverages on 16 February 2000 and 9 February 1962; a detailed comparison of these provides an estimate of the thinning of the ice fields over the last 38 years. Ground control for the 2000 map consisted of 11 Global Positioning System (GPS) positions (*5*), and control for the restitution of the 1962 photography was obtained by transferring fixed points common to the two sets of photos from the 2000 photography. This comparison yields an average surface lowering of ~17 m over this 38-year period or an average thinning of ~0.5 m per year for Kilimanjaro's ice cover. Total ice area calculated from successive maps (1912, 1953, 1976, 1989, and 2000) reveals (Fig. 1, inset) that the areal extent of Kilimanjaro's ice cover has decreased approximately 80% from ~12 km^2 in 1912 to ~2.6 km^2 in 2000 and that since 1989, a hole has developed near the center of the NIF. A nearly linear relationship (R^2 = 0.98) suggests that if climatological conditions of the past 88 years continue, the ice on Kilimanjaro will likely disappear between 2015 and 2020.

The chemical and physical analyses, coupled with visible stratigraphy for near-surface layers of the NIF2 core, are shown in fig. S1A. Melt features similar to those in the top meter did not occur elsewhere in the NIF or SIF cores. The ongoing down-wasting of the ice fields had not yet removed the ice deposited in the early 1950s, because snow was recovered that contained elevated concentrations of ^{36}Cl from the 1952 Ivy thermonuclear bomb test on Eniwetok Atoll (*6*). The 1952 time horizon, used for time control in other low-latitude ice cores (see fig. S1B), provided a logical origin for development of a depth-age model for the suite of Kilimanjaro cores.

The δ^{18}O records in the five cores displayed significant similarity, including numerous distinctive horizons that provided a means of continuous cross-correlation even though the temporal sequences they represent are of differing lengths. Depth-to-depth transfer (referencing all cores to NIF3) involved linear interpolation between consecutive match points (*7*) spaced uniformly throughout the records. Rescaling of the NIF2 δ^{18}O profile (Fig. 2B) to the NIF3 depth scale (Fig. 2C), as well as the SIF1, SIF2, and FWG δ^{18}O profiles, establishes that NIF3 contains the longest record, with the information preserved in the bottom 17.5 m absent in the other cores. Defining time scales for the five cores required constructing a time scale for NIF3 and then referencing the other four cores to this master chronology through the depth-to-depth transfers already generated. We used the simplest age modeling for a steady-state glacier of constant accumulation (supporting online text), the formula introduced by Nye (*8*) and later time-integrated for application to ice cores in Greenland (*9*). Hence, the precise timing of climate events inferred from the Kilimanjaro cores cannot be considered absolute, based on our assumptions of a consistent ice thickness (roughly 50 m) and an invariant accumulation rate for model age control.

Application of the model required estimating a representative annual accumulation rate that is assumed to remain constant. Three time horizons (supporting online text) were chosen to guide a finite approximation of the Nye model to NIF3. In addition to the 1952 horizon and the estimated age at bedrock [~11.7 thousand years, discussed below], an age of 1325 A.D. was assigned to the center of the large, sustained ^{18}O depletion (Fig. 2, event 2) at 8.50 m in NIF3 (9.82 m in NIF2). Water levels in Lake Naivasha, Kenya (Fig.

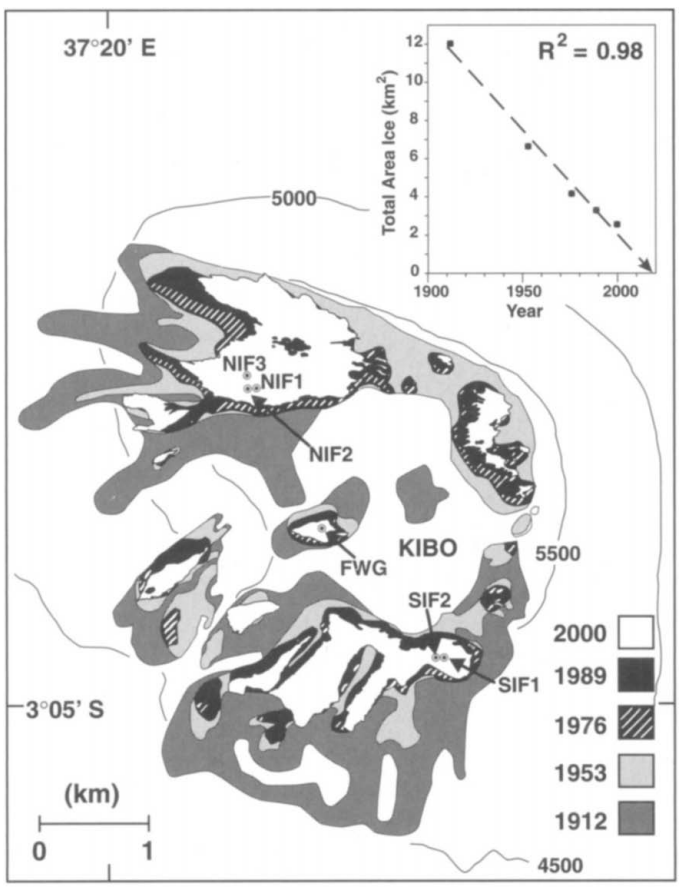

Fig. 1. Shown are the outlines of the Kibo (Kilimanjaro) ice fields in 1912, 1953, 1976, and 1989 (*3*) updated to 2000 using the OSU aerial photographs taken on 16 February 2000. The insert illustrates the nearly linear decrease in ice area from 1912 to 2000.

3), show higher stands during all three recent solar minima (Maunder, Spörer, and Wolf) with a ~100-year (1670 to 1780 A.D.) period of overflow coincident with the Maunder Minimum. The earliest of the three high stands of Lake Naivasha is ^{14}C-dated between 1290 and 1370 A.D., and the close association between the water balance in East Africa and solar variability (*10*) argues for a relationship between the NIF $\delta^{18}O$ minima and the solar minima (Fig. 3). In light of the support from other proxy evidence, the central age of the Wolf Minimum (1325 A.D.) was assigned to the earlier and deeper of the two large $\delta^{18}O$ depletions (event 2 in Fig. 2) in the Kilimanjaro cores (supporting online text).

A radiocarbon age of 8.28 ± 0.38 thousand years [9.36 ± 0.47 thousand calendar years before 1950 A.D. ($^{14}C_{cal}$ years) (*11*)] determined from small quantities of organic samples from the deepest section (47.9 to 49.0 m) of NIF3 supports the presence of early Holocene ice (table S1). The absence of Late Glacial Stage (LGS) ice is inferred from the lack of strong [≥5 per mil (‰)] isotopic depletion at the bottom of NIF3 that characterizes LGS ice in both polar and nonpolar cores (*12*). A Holocene age for NIF3 formation required development of a finite approximation (supporting online text) to the age-depth relationship near the bottom of the core. A basal age of 11.7 thousand years was assigned by comparing the NIF3 $\delta^{18}O$ record with the precisely dated [^{230}Th–^{234}U by thermal ionization mass spectrometry] $\delta^{18}O$ speleothem record from Soreq Cave (Fig. 4, C and D) in the eastern Mediterranean region (*13*).

The Kilimanjaro ice cores provide a nearly continuous, high-resolution record of Holocene climate conditions. The 50-year averages of $\delta^{18}O$ and insoluble dust are shown along with several other proxy records for the past ~11.7 thousand years (Fig. 4). Isotopic enrichment (indicating warmer conditions) and reduced concentrations of major aerosol species (Mg^{2+}, Ca^{2+}, SO_4^{2-}, and NO_3^-, indicating wetter conditions) dominate from ~11 to 4 ka. These indicate ice that formed during the well-documented African Humid Period (~11 to 4 ka), when warmer and wetter conditions prevailed (*14*, *15*) in response to the precession-driven increase in solar radiation (*16*). During this interval, lakes in the region rose as much as 100 m above present levels (*14*, *17*), and in sub-Saharan Africa lake expansion was massive, with Lake Chad expanding 25-fold from ~17,000 km^2 to cover an area between ~330,000 and 438,000 km^2, comparable to that of the Caspian Sea today (*14*, *18*, *19*). A paleolake filled the Magadi Natron basin on the border between Tanzania and Kenya to a depth 50 m above the present level and had an area of ~1600 km^2 in the early Holocene (*20*). Calculations of the hydrological balance (*21*) suggest that annual precipitation over the Lake Chad Basin was as high as 650 mm, compared with 350 mm today, and mean precipitation over the Ziway-Shala Basin in Ethiopia was similarly calculated (*17*) to be 47% higher than today. After ~4 ka, African lake levels dropped as conditions became cooler (more depleted in ^{18}O) and drier (more elevated peak concentrations of the major aerosol species) (Fig. 4 and fig. S2). The Kilimanjaro records capture the major African climate trends during the Holocene, as well as the larger scale trends in tropical temperature, as shown by their similarity to the Huascarán $\delta^{18}O$ and dust records (Fig. 4, B and G) (*22*).

The Kilimanjaro record documents three abrupt climate changes in this region: at ~8.3, ~5.2, and ~4 ka. Unlike the major aerosol concentrations discussed above, F^- and Na^+ concentrations are sporadically high from ~11 to 4 ka and low during the past ~4

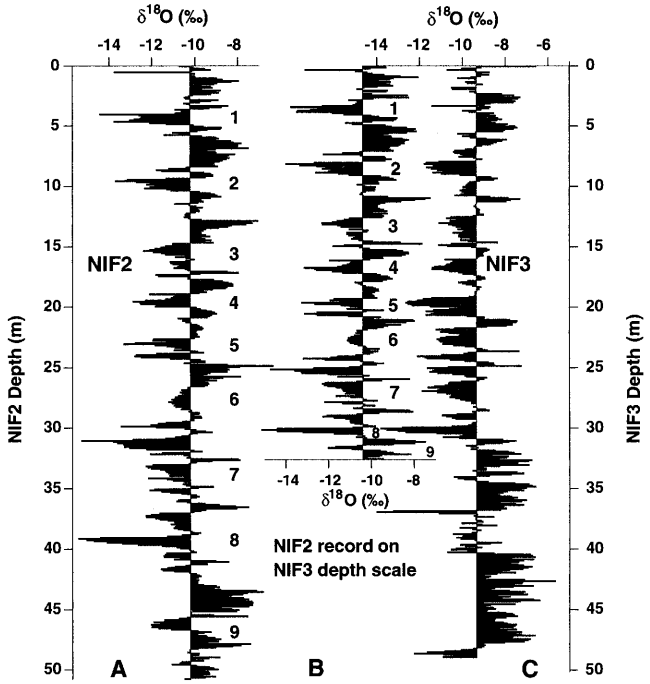

Fig. 2. (**A** and **C**) The 10-year average $\delta^{18}O$ records from the (A) NIF2 and (C) NIF3 cores are shown for their entire lengths. (**B**) NIF2 depths are rescaled to the NIF3 depth scale by matching similar $\delta^{18}O$ features, showing that NIF2 is contemporaneous with the upper 32 m of NIF3. The $\delta^{18}O$ events labeled 1 to 9 are assumed to be coeval.

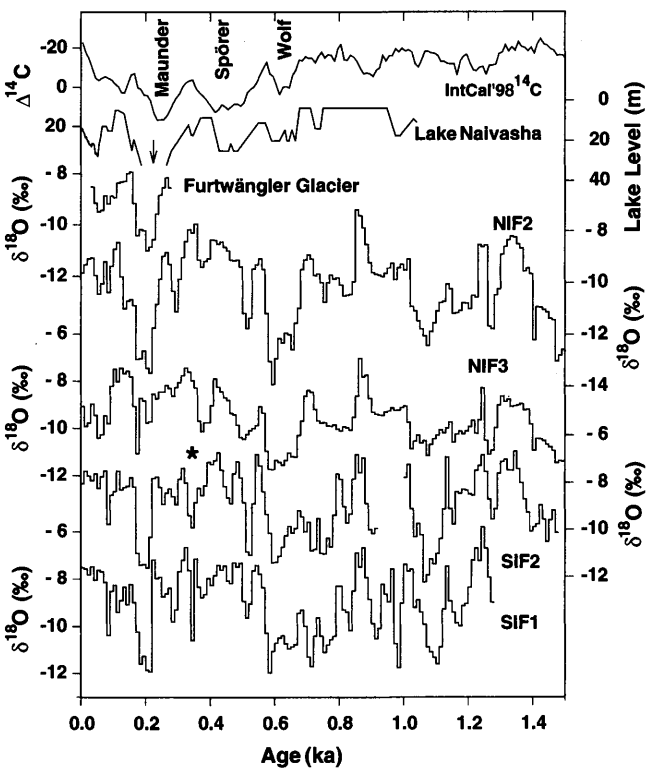

Fig. 3. The decadal averages of $\delta^{18}O$ from five cores drilled to bedrock are compared with the high-resolution lake level record from Lake Naivasha (*10*) and with the decadal record of atmospheric ^{14}C (*11*) that was used as a proxy for solar variability. The one section of missing data in the SIF2 plot reflects a meter of core that was damaged during transport down the mountain. The asterisk on SIF2 indicates a 6-m section of anomalous ice (supporting online text).

thousand years. The F^- concentrations between ~8.4 and 8.2 ka (fig. S2) are the highest yet reported from an ice core. These high levels are concurrent with the large, abrupt reduction in methane (CH_4) at ~8.2 ka in the European Greenland Ice Core Program (GRIP) core (*23*) and with the greatest Holocene depletion of ^{18}O in both the GRIP and the Greenland Ice Sheet Project 2 records (*24*). These aerosol spikes are interpreted as intermittent periods of rapidly fluctuating lake levels from ~11.7 to 5 ka (*17*) within the longer period of overall high lake stands (Fig. 4A). The volcanic rocks of the East Africa Rift Valley are mainly alkaline basalt, basanites, and tephrites rich in Na^+ and containing higher concentrations of F^- than analogous rocks in other parts of the world (*25*). The products of weathering of these rocks, when deposited in evaporating lakes, form an F^--rich salt crust or trona (*26*, *27*), known locally as magadi. For example, Lake Magadi in the Kenya Rift Valley is covered by a trona layer with high concentrations of F^-. Periods of high runoff would concentrate sodium and fluoride in the lakes, and when lake levels declined, trona would be precipitated as land surfaces dried. This process provides abundant sources of F^--enriched trona that can be eroded and entrained into the local background aerosol, thus becoming part of the regional aerosol history preserved in the Kilimanjaro ice fields (fig. S2). The highest sustained levels of F^- and Na^+ [1110 and 1957 parts per billion (ppb), respectively] occur at ~8.3 ka and likely reflect a large rapid drop in lake levels (e.g., a brief but strong drying period) in the region. Within the limits of dating errors in both records, the contemporaneity of these F^- and Na^+ pulses in the Kilimanjaro ice core and the global reduction in CH_4 inferred from the GRIP ice core (independent time scales) strongly suggest that the ~8.2 ka CH_4 event was driven by abrupt and large hydrologic changes in the tropics, particularly in Africa.

The second large event in the Kilimanjaro record began as an abrupt ^{18}O depletion at ~6.5 ka that continued for more than a millennium. It culminated as a sharp dip of > 5‰ at ~5.2 ka (Fig. 4D) that was followed by rapid recovery and sustained ^{18}O enrichment from ~5 to 4 ka. The cooling indicated by the more negative $\delta^{18}O$ values from ~6.5 to 5 ka is coincident with a "second humid period" (~6.5 to 4.5 ka) when conditions were wetter than today but drier than the early Holocene "first humid period" (*15*). During this second humid period, the Ziway-Shala Basin attained its highest levels (~6.0 to 5.5 ka) (Fig. 4A) before dropping rapidly (beginning ~5.5 ka) to near modern low levels by ~4 ka. The abrupt cooling event ~5.2 ka is recorded as the largest ^{18}O depletion in Kilimanjaro ice and the largest ^{18}O enrichment in the Soreq cave record (Fig. 4, C and D). This climatic change recorded in Kilimanjaro ice is concomitant with a decline in both lake levels (*14*, *28*, *29*) and vegetative cover (*30*), as well as the lowest CH_4 concentrations in Holocene ice from Greenland (*23*). The change of climate is also consistent with documentary evidence ranging from northern Africa to Arabia (*31*). Almost contemporaneously, at ~5.3 ka, hierarchical societies formed in the over-populated Nile Valley and Mesopotamia, while Neolithic settlements in the inner desert of Arabia were abandoned (*28*). This century-scale rapid cooling and drying event correlates with the 5.2-ka Late Uruk abrupt climate change that is suggested to have altered environments and subsistence outside the Mesopotamian lowlands (*31*).

The third abrupt climate event recorded in Kilimanjaro ice is associated with the most distinct visible dust layer, 30 mm thick, in NIF3 at 32.53 m (Fig. 4E). This layer also contains high concentrations of other chemical species (fig. S2 and table S2) and may represent a hiatus in mass accumulation of undetermined length. Isotopic matching of NIF2 and NIF3 (Fig. 2, B and C) correlates the bottom of the NIF2 record (~4 ka) with the deposition of this dust layer preserved in NIF3. This date for the bottom of NIF1 and NIF2 is generally supported by two ^{14}C dates [4050 (3781 to 4351) and 6090 (5906 to 6281) $^{14}C_{cal}$ years] measured on very small amounts of material in the bottom (50.01 to 51.03 m) of NIF1 (table S1). The absence of the thick visible dust layer in the NIF1 and NIF2 cores suggests that, at ~4 ka, the NIF was smaller than it is today and that the crater-side ice wall likely retreated past the present-day sites of NIF1 and NIF2. Thus, it appears that the major dust layer at 32.5 m in NIF3 was deposited during extremely dry conditions either before or during the retreat of the NIF margin.

There is abundant ancillary evidence for the dry climate at this time. Water levels were very low in the lakes of tropical east Africa (*17*), and the effects of this drought were experienced throughout northern and tropical Africa, the Middle East, and western Asia (*17*, *32*, *33*). This drought event was so severe that it has been considered instrumental in the collapse of a number of civilizations (*34*). The regional coincidence of low lake levels, reduction of ice cover on Kilimanjaro, deposition of a thick layer of dust, and societal upheaval suggest a large climate event centered at ~4 ka. Further evidence for the regional extent of the event is recorded by an increase in dolomite in a sediment core from the Gulf of Oman (*35*) at this time (Fig. 4F). The possibility that the drought was much more extensive is suggested by the contemporaneity of the Kilimanjaro dust event with an enormous dust event recorded in ice cores from Huascarán in the Andes of Northern Peru (*22*) at ~4.3 ka (Fig. 4G, note scale change). Evidence for the end of this arid period is abundant (supporting online text). As the ~300-year-long drought ameliorated (*35*), the NIF would necessarily begin to accumulate mass and reestablish itself over a larger portion of the crater rim, including the part of the ice field from which the NIF 1 and 2 cores were drilled.

Kilimanjaro's remaining ice fields are Ho-

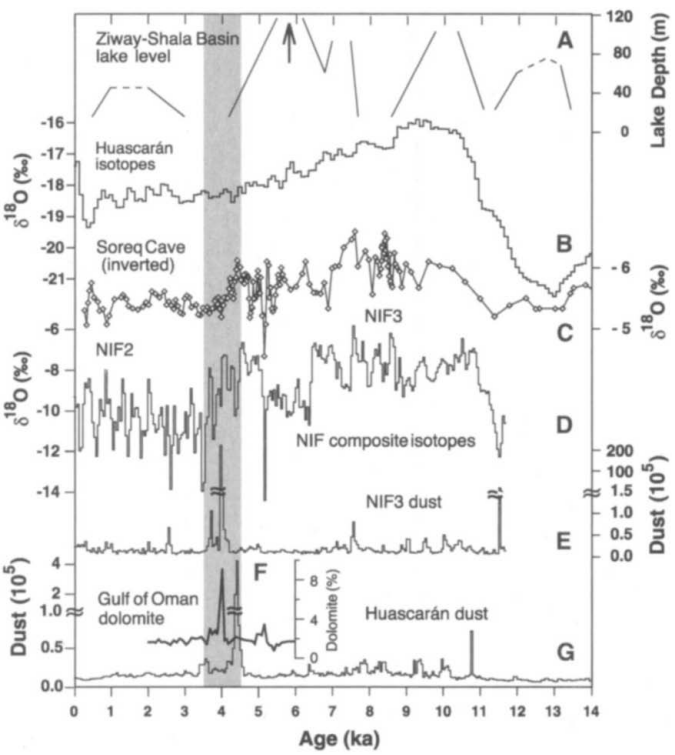

Fig. 4. (**A** to **G**) The 50-year averages of the Holocene $\delta^{18}O$ and dust histories from Kilimanjaro ice cores are compared with other proxy records as discussed in the text. The Huascarán dust and $\delta^{18}O$ plots are also 50-year averages, and all dust concentrations are for particles with diameters from 0.63 to 16.0 μm per ml sample. Vertical gray shading indicates the period of drought during the First Dark Age.

locene features that have expanded and contracted in concert with the large-scale warming and cooling phases of the Holocene in Africa. The ice core records from the SIF and FWG indicate that ice cover on Africa's highest mountain has varied through the Holocene. The FWG appears to have formed only in the past few centuries, likely at the onset of the coldest part of the most recent Neoglacial or Little Ice Age period. We speculate that the FWG is an ephemeral feature, unlike the larger rim ice fields that have been more persistent through time.

Model-derived dates, coupled with ^{14}C ages for the bottom ice in the NIF, suggest that it began to grow ~11.7 ka and expanded during the African Humid Period. Clearly there was less ice on the summit of Kilimanjaro at ~4 ka, coincident with the "First Dark Age," the period of the greatest historically recorded drought in tropical Africa, which apparently extended to the Middle East and western Asia. The disappearance of Kilimanjaro's ice fields, expected between 2015 and 2020, will be unprecedented for the Holocene. This will be even more remarkable given that the NIF persisted through a severe ~300-year drought that so disrupted the course of human endeavors that it is detectable from the historical and archaeological records throughout many areas of the world. A comparison of the chemical and physical properties preserved in the NIF with those in the water-saturated, rapidly shrinking FWG (*36*), coupled with the lack of melt features in the NIF and SIF cores, confirms that conditions similar to those of today have not existed in the past 11 millennia. The loss of Kilimanjaro's permanent ice fields will have both climatological and hydrological implications for local populations, who depend on the water generated from the ice fields during the dry seasons and monsoon failures.

References and Notes

1. Equipment description and data are available at www.geo.umass.edu/climate/kibo.html.
2. S. E. Nicholson, in *The Limnology, Climatology and Paleoclimatology of the East African Lakes*, T. C. Johnson, E. O. Odada, Eds. (Gordon and Breach, Amsterdam, 1996), pp. 25–56.
3. S. Hastenrath, L. Greischar, *J. Glaciol.* **43**, 455 (1997).
4. B. Messerli, *IAHS-AISH Publ.* **126**, 197 (1980).
5. The 11 GPS positions were obtained from three different sources: two points of geodetic (cm) accuracy from a joint Tanzanian-German survey in September 1999 (*37*), seven points with accuracies of 2 to 5 m from surveys by D.R.H. and colleagues in February and June 2001, and two points of low accuracy (15 to 20 m) established by the Ohio State University (OSU) field party in February 2000, all weighted accordingly.
6. M. W. Carter, A. A. Moghissi, *Health Phys.* **33**, 55 (1977).
7. D. Palliard, L. Labeyrie, P. Yiou, *EOS* **77**, 379 (1996).
8. J. F. Nye, *J. Glaciol.* **4**, 785 (1963).
9. W. Dansgaard, S. J. Johnsen, *J. Glaciol.* **8**, 215 (1969).
10. D. Verschuren, K. R. Laird, B. F. Cumming, *Nature* **403**, 410 (2000).
11. M. Stuvier, P. J. Reimer, T. F. Braziunas, *Radiocarbon* **40**, 1127 (1998).
12. L. G. Thompson *et al.*, *Science* **282**, 1858 (1998).
13. M. Bar-Matthews, A. Ayalon, A. Kaufman, G. J. Wasserburg, *Earth Planet. Sci. Lett.* **6**, 85 (1999).
14. F. A. Street, A. T. Grove, *Quat. Res.* **12**, 83 (1976).
15. S. E. Nicholson, H. Flohn, *Clim. Change* **2**, 313 (1980).
16. J. E. Kutzbach, F. A. Street-Perrott, *Nature* **317**, 130 (1985).
17. F. A. Street-Perrott, R. A. Perrott, *Nature* **343**, 607 (1990).
18. A. T. Grove, A. Warren, *Geogr. J.* **134**, 194 (1968).
19. A. Broström *et al.*, *Geophys. Res. Lett.* **25**, 3615 (1998).
20. C. Hillaire-Marcel, J. Casanova, *Palaeogeogr. Palaeoclimatol. Palaeocol.* **58**, 155 (1987).
21. J. E. Kutzbach, *Quat. Res.* **14**, 210 (1980).
22. L. G. Thompson, E. Mosley-Thompson, K. A. Henderson, *J. Quat. Sci.* **15**, 377 (2000).
23. T. Blunier, J. Chappellaz, J. Schwander, B. Stauffer, D. Raynaud, *Nature* **374**, 46 (1995).
24. R. B. Alley *et al.*, *Geology* **25**, 483 (1997).
25. P. Kilham, R. E. Hecky, *Limnol. Oceanogr.* **18**, 932 (1973).
26. J. T. Nanyaro, U. Aswathanarayana, J. S. Mungure, *J. Afr. Earth Sci.* **2**, 129 (1984).
27. S. J. Gaciri, T. C. Davies, *J. Hydrol.* **143**, 395 (1993).
28. F. Sirocko *et al.*, *Nature* **364**, 322 (1993).
29. F. A. Street-Perrott, J. F. B. Mitchell, D. S. Marchant, J. S. Brunner, *Trans. R. Soc. Edinburgh Earth Sci.* **81**, 407 (1990).
30. A. M. Swain, J. E. Kutzbach, S. Hastenrath, *Quat. Res.* **19**, 17 (1983).
31. H. Weiss, in *Environmental Disaster and the Archeology of Human Response*, G. Bawden, R. M. Reycraft, Eds. (Anthropological Papers, No. 7, Maxwell Museum of Anthropology, University of New Mexico, Albuquerque, 2001), pp. 75–95.
32. H.-J. Pachur, P. Hoelzmann, *J. Afr. Earth Sci.* **30**, 929 (2000).
33. F. Gasse, E. Van Campo, *Earth Planet. Sci. Lett.* **126**, 435 (1994).
34. H. N. Dalfes, G. Kukla, H. Wiess, *Third Millennium BC Climate Change and Old World Collapse* (NATO ASI Series I: Global Environmental Change, vol. 49, Springer, Berlin, 1994).
35. H. M. Cullen *et al.*, *Geology* **28**, 379 (2000).
36. The ion concentrations from the water-saturated FWG (~1670 to 1920 A.D.) were compared with those measured in the NIF cores for the same time interval to support our contention that the NIF has not been water-saturated (measurements of FWG versus NIF, all in ppb: F^-, 3.3 versus 5.8; NO_3^-, 59.6. versus 255.5; SO_4^{2-}, 22.1 versus 69.4; Na^+, 31.6. versus 126.8; K^+, 8.9 versus 38.2; Mg^{2+}, 1.5 versus 4.9; and Ca^{2+}, 8.2 versus 42.1).
37. J. Saburi *et al.*, *Survey Rev.* **35**, 278 (2000).

38. This project was funded by grant ATM-9910172 from the NSF's Earth System History Program. We thank M. Illner of the Geodetic Institute of the University of Karlsruhe (GIK) for providing positions and helping to locate the points of the survey carried out by a party with participants from GIK; Karlsruhe University of Applied Science; University College of Lands and Architectural Studies; the Surveys and Mapping Division, Tanzania; and Leica Geosystems. We thank R. Fox, International Library Manager, U.K. Ordnance Survey, for his help in searching for existing old photography and ground control points. Photomap (Kenya) Ltd. did an excellent job of taking our February 2000 aerial photographs. The Accelerator Mass Spectrometry (AMS) ^{14}C dates were measured by T. Guilderson of The University of California's Lawrence Livermore National Laboratory and by the National Ocean Sciences AMS Facility at Woods Hole Oceanographic Institution. We thank P. R. Edwards for the analytical chemistry measurements he made on NIF3 while he was a Byrd Postdoctoral Fellow. We are indebted to P. Ndesamburo and the staff of the Key's Hotel who facilitated securing the many permits and making logistical arrangements in Tanzania and to J. Minja (chief guide) and the 92 porters who made this project possible. This is Byrd Polar Research Center contribution number 1264.

Supporting Online Material

www.sciencemag.org/cgi/content/full/298/5593/589/DC1
Supporting Text
Figs. S1 and S2
Tables S1 and S2
References and Notes

23 April 2002; accepted 3 September 2002

A Primordial Origin of the Laplace Relation Among the Galilean Satellites

S. J. Peale* and Man Hoi Lee

Understanding the origin of the orbital resonances of the Galilean satellites of Jupiter will constrain the longevity of the extensive volcanism on Io, may explain a liquid ocean on Europa, and may guide studies of the dissipative properties of stars and Jupiter-like planets. The differential migration of the newly formed Galilean satellites due to interactions with a circumjovian disk can lead to the primordial formation of the Laplace relation $n_1 - 3n_2 + 2n_3 = 0$, where the n_i are the mean orbital angular velocities of Io, Europa, and Ganymede, respectively. This contrasts with the formation of the resonances by differential expansion of the orbits from tidal torques from Jupiter.

The orbital resonances among the Galilean satellites of Jupiter have led to sustained dissipation of tidal energy to produce astounding volcanos on Io and, probably, to maintain a liquid ocean on Europa. Understanding the origin of these resonances will constrain the history of the satellites and their formation scenarios. The two models proposed are an assembly of the resonances through differential tidal expansion of the orbits from tides raised on Jupiter (*1*, *2*) and a primordial origin of unspecified assembly and subsequent evolution away from exact resonance (*3*, *4*). Here we discuss a means of

Department of Physics, University of California, Santa Barbara, CA 93106, USA.

*To whom correspondence should be addressed. E-mail: peale@io.physics.ucsb.edu